Case Studies in Construction Materials 6 (2017) 162–176

Contents lists available at ScienceDirect

Case Studies in Construction Materials

journal homepage: www.elsevier.com/locate/cscm

Short communication

Acoustic emission characteristics of reinforced concrete beams with varying percentage of tension steel reinforcement under flexural loading

R. Vidya Sagar

Department of Civil Engineering, Indian Institute of Science, Bangalore, 560 012, India

ARTICLE INFO

Article history:
Received 16 September 2016
Received in revised form 10 January 2017
Accepted 10 January 2017
Available online 16 January 2017

Keywords:
Reinforced concrete
Acoustic emission
Damage
Cyclic loading
Structural health monitoring

ABSTRACT

Reinforced concrete (RC) flanged beam specimens were tested under incremental cyclic load till failure in flexure. Simultaneously the acoustic emissions (AE) known as transient elastic stress waves released during fracture process in the same specimens were recorded. These RC flanged beam specimens were cast with different percentage of steel reinforcement (area of steel reinforcement as a percentage of the effective area of beam cross section). Crack widths depend on tensile stress in steel reinforcement present in a RC structural member. Because crack opening is a function of tensile stress in the steel rebars, the percentage of steel in the RC members influence the AE released during fracture process. In this article, a study on damage occurred in RC flanged beam specimens having different percentage of steel reinforcement using acoustic emission testing is reported. A relation between the total AE energy released and percentage of steel in RC beams has been proposed. As the percentage of steel present in the test specimen was increased, the loading cycle number entering into the heavy damage zone in NDIS-2421 damage assessment chart also increased.

1. Introduction

Limiting the crack width in RC structural members is related to the serviceability limit state conditions and is also an important concern. The minimum reinforcement in a RC member is governed by crack width. In serviceability limit state condition to avoid unstable fracture process and hyper-strength phenomenon minimum reinforcement in a RC structural member is required [1]. Minimum area of tension reinforcement (A_s) in a flanged RC beam shall not be less than $\frac{0.85b_w d}{f_y}$, where b_w is breadth of the web of a T- beam, d is effective depth and f_y is characteristic strength of reinforcement [2]. Also the Indian code of practice for plain and reinforced concrete IS:456-2000 recommends that maximum area of tension steel or compression steel shall not exceed $0.04b_wD$ where D is the overall depth of the flanged beam [2].

Cracking of concrete is not supposed to affect the appearance or durability of the RC structure. The acceptable limits of crack widths differ with the type of structures and the surrounding environment. In case of some RC structures specific attention is required to limit the crack width to a specified value. In general, the surface width of cracks should not exceed 0.3 mm in RC structural members. When the crack width exceeds 0.3 mm, the RC structure is unsafe [2]. Also crack width should not have any serious adverse effect upon the preservation of reinforcing steel nor upon the durability of the structure.

E-mail address: rvsagar@civil.iisc.ernet.in (R. Vidya Sagar).

http://dx.doi.org/10.1016/j.cscm.2017.01.002

In RC structural members where cracking in the tension zone is harmful due to expose to the effect of the weather, continuously exposed to moisture, in contact with soil, ground water an upper limit of 0.2 mm is suggested for the minimum width of cracks [2].

2. Research significance

Large number of RC structures including the residential buildings, bridges, commercial buildings, water tanks in India have surpassed their service life and this raises the need for the rehabilitation of these RC structures. This demands a proper damage assessment. Because deterioration is a natural phenomenon and the deterioration has started in these existing RC structures. Therefore non-destructive testing (NDT) of *in-service* RC structures is required to locate the ongoing fracture process. AE monitoring technique which is a NDT method is useful for real time damage detection of RC structures [3].

3. Literature review

Over the past few years, researchers have attempted to study the state of the damage in the existing RC structures using parameter based AE techniques. Several attempts have been made to study the fracture properties of concrete using AE monitoring techniques [3] and recently Ohtsu edited AE and related NDT techniques in context of fracture mechanics of concrete, which consolidates the recent developments in application of AE monitoring technique to study fracture process in concrete structures [4]. Also, Behnia et al. reviewed application of AE monitoring techniques to the concrete structures [5]. Ohtsu et al. used AE energy and the Kaiser effect phenomenon to study the state of damage in RC beams in laboratory under incremental cyclic loading [6]. Colombo et al. and several other researchers used AE based *b*-value which is based on the Gutenberg-Richter empirical relation to study the fracture process in RC beams and concluded that the variation in *b*-value showed a relationship with micro-cracking and macro-cracking [7–9]. Vidya Sagar and Rao studied the effect of loading rate on the variation in AE based *b*-value related to RC structures [8]. Ridge and Ziehl used the AE parameter signal strength to evaluate the damage in concrete specimens [10]. Nair and Cai used intensity analysis to assess damage in concrete bridges *in-stu* [11]. And several researchers extensively studied AE monitoring techniques applicable to concrete structures [12–21]. The AE released during fracture process dependence on the crack width and crack opening in RC structures. Because crack opening is a function of tensile stress in the steel rebars present in RC structures. Hence the percentage of steel in the RC structural members influence the acoustic emissions released and the damage.

4. Evolution of the shear and tensile cracks during loading

The Gaussian mixture modeling is a multivariate probabilistic analysis which allows the user to sort large quantity of data into different clusters using the Expectation – maximization algorithm. In order to classify the data into tensile and shear crack clusters, the GMM method has been used. The GMM or the linear superposition of Gaussians is given in Eq. (1) [3,5,28].

$$p(x) = \Sigma_{k=1}^{K} \pi_k N(x|\mu_{k,} \sum{}_k) \tag{1}$$

Where K is the number of Gaussians and k = 1, ... · · ·K, $N(x|\mu_{k,} \sum{}_k)$ is the normal multivariate Gaussian distribution for class K, π_k is the mixing coefficient or the weightage for each Gaussian distribution. A D-variate Gaussian distribution function is given in Eq. (2)

$$N\left(x|\mu_{k,} \sum{}_k\right) = \frac{1}{(2\pi)^{D/2} |\sum|^{1/2}} e^{\frac{-1}{2}\left[(x-\mu)^T \sum^{-1} (x-\mu)\right]} \tag{2}$$

μ_k is the vector form of mean for the kth Gaussian, $\sum_k$ v is the covariance matrix for the kth Gaussian. The mixing coefficient or the weightage, satisfies the constraint $0 \leq \pi_k \leq 1$ and

$$\Sigma_K^K \pi_k = 1 \tag{3}$$

The details about Gaussian mixture modeling are given in [28].

5. Aim of the present study

AE monitoring technique is a useful nondestructive evaluation technique to assess the damage condition in real time of existing RC structures in-service. However, this experimental technique's consistency is not well established. Several studies were conducted on fracture monitoring using AE monitoring technique. In some practical cases, reinforcement steel is reduced below the specified steel due to inability in execution by engineers working *in-situ*. The study present in this article examines the characteristics of AE released during fracture process in RC beams with varying percentage of steel reinforcement and also the damage status.

Table 1
Geometric details and material properties of RC flanged beam specimen.

Specimen	Ø (mm)	n	A_s (mm^2)	S (mm)	L (mm)	W_f (mm)	D (mm)	b_w (mm)	d_w (mm)	Percentage of tension steel (P) (%)
SPB1a	20	4	1256	2600	3210	500	560	180	380	1.45
SPB1b	20	4	1256	2600	3210	500	560	180	380	1.45
SPB1c	20	4	1256	2600	3210	500	560	180	380	1.45
SPB2	20	3	942	2600	3210	500	560	180	380	1.06
SPB3	20	2	628	2600	3210	500	560	180	380	0.75

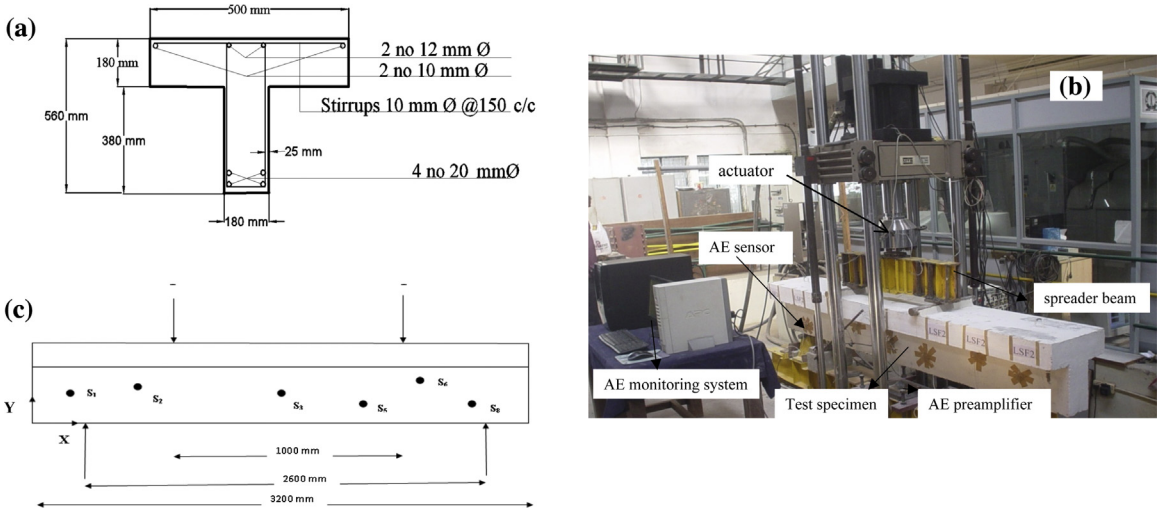

Fig. 1. a: Schematic diagram of the geometric properties and steel reinforcement details in the flanged beam specimen; b: RC flanged beam specimen instrumented with AE sensors for fracture monitoring in the test rig, Structures laboratory, Department of Civil Engineering, Indian Institute of Science, Bangalore, India; c: Schematic representation of AE sensor locations on the test specimen.

6. Experimental program

6.1. Materials and test specimens

Five RC flanged beam specimens of 3.2 m length and 2.6 m span were tested and details are given in Table 1. In the same table, in specimen name SPB1, '*S*' stands for steel, '*P*' stands for percentage and 'B' indicates beam. '1' indicates the test specimens having 1.45 percentage of tensile steel. Similarly for the test specimens SPB2 and SPB3, '2' indicates 1.06 percentage of tensile steel and '3' indicates 0.75 percentage of tensile steel respectively.

Experiments were conducted using three specimens each having 1.45 percentage of tension steel and a single specimen for test specimen containing 1.06 and 0.75 percentage of steel respectively. The geometry and steel reinforcement details are given in Table 1 and in the same table φ is nominal diameter of tensile steel bar; n is number of tensile reinforcement bars; A_s is the area of reinforcement which is equal to $\left[nX\frac{\pi}{4}\varphi^2\right]$; p is the area of steel reinforcement as a percentage of the effective area of beam cross section and is equal to $\left(\frac{A_s}{b_w D}X100\right)$; L is the length of the flanged beam; S is span of the flanged beam; b_w is the width of the flanged beam rib (or web); D is beam the overall depth of the flanged beam. The details about the fixation of test specimen dimensions are given in [22]. All RC flanged beam specimens with different percentage of tension steel (1.45%,

Table 2
AE sensor location coordinates [2D XY planar].

Specimen	Sensor location (mm) [2D planar]											
	1		2		3		5		6		8	
	X	Y	X	Y	X	Y	X	Y	X	Y	X	Y
SPB1a	1000	270	2200	140	2810	200	360	100	2440	370	1600	200
SPB1b	460	300	900	240	1600	175	2000	160	2400	210	2800	190
SPB1c	460	240	800	225	1200	200	2000	160	2400	210	2800	190
SPB2	460	300	900	240	1600	200	2000	160	2400	210	2800	190
SPB3	420	180	920	220	1600	200	2000	120	2500	190	2800	210

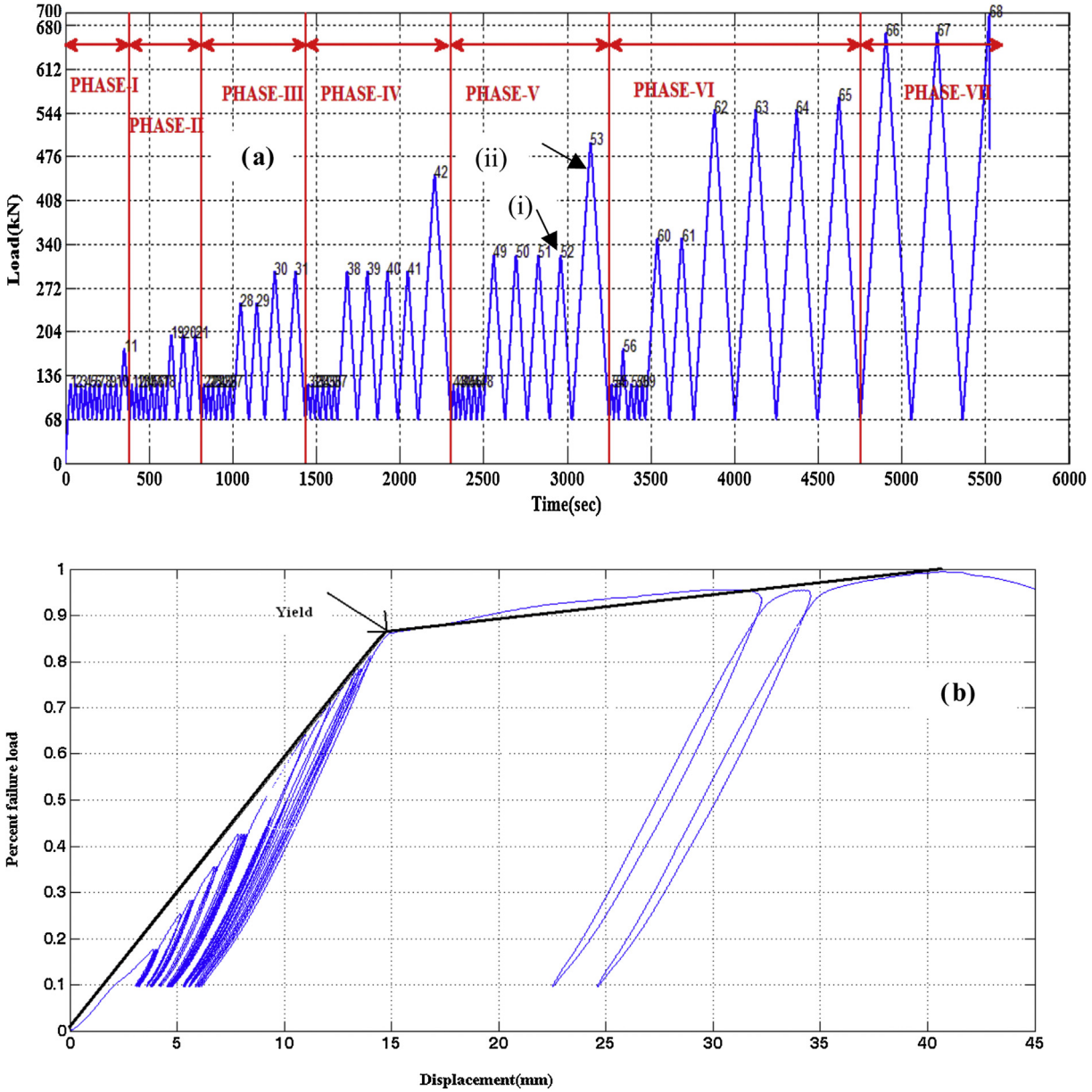

Fig. 2. (a) Loading protocol applied to SPB2 specimen. (i) transport vehicle load (ii) elevated test truck load. Recorded plots of (b) percent failure load versus mid-span displacement (c) load versus displacement (d) Variation of strain in tensile steel with time.

1.06% and 0.75%) with same span and depth as shown in Fig. 1a was tested in four point bending. Normal strength concrete (37 MPa, maximum coarse aggregate size is 20 mm) was used for preparation of the test specimens. A schematic diagram of the reinforcement details are shown in Fig. 1a.

6.2. Experimental arrangement

The experimental setup consisted of a servo hydraulic loading machine (maximum capacity of 1200 kN) with a data acquisition facility and the AE monitoring system. A steel beam (I- cross section) was placed beneath the hydraulic loading machine's actuator to transfer the total load at two points on the test specimen as shown in Fig. 1b. Two-point loading span was 1 m with 2.6 m supporting-span. The released AE signals were recorded simultaneously using a 8 channel AE monitoring system. The mid-span displacement was measured using a linearly varying displacement transducer placed at the center on the underside of the specimen. The strain in steel at mid section of the test specimen was recorded using an120 Ω electrical-resistance strain gauge.

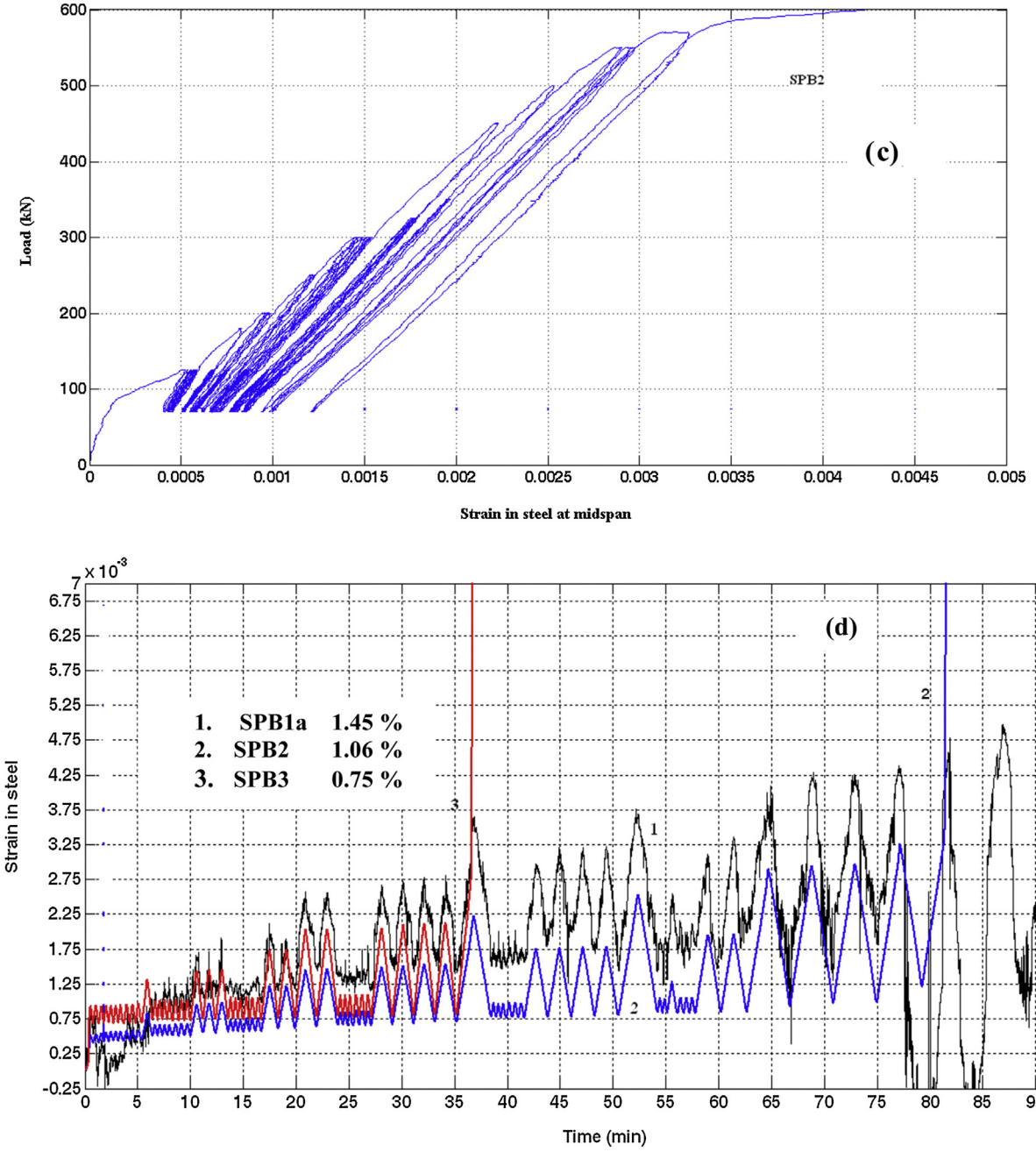

Fig. 2. (Continued)

6.3. AE instrumentation

The AE sensors (resonant type) are mounted on the test specimen using a 2D location pattern. The AE sensor has peak sensitivity at 57 dB with reference to 1 V/(m/s). The operating frequency of the AE sensor was 35 kHz–100 kHz. The used differential resonant type AE sensor has a good sensitivity and frequency response over the range of 35 kHz–100 kHz. The sensor has a resonant frequency of approximately at 57 kHz. The response was nearly same for all the resonant sensors used in this experimental study. The threshold value of 40 dB was selected to ensure a high signal to noise ratio. The total AE energy released was calculated by summing up the AE energy recorded by the used 6 channels. The AE sensor's location on the test specimen is shown in Fig. 1c schematically and also the coordinates of the senor location was given in Table 2.

Table 3
Recorded downward displacement, strain in steel at mid-span and AE parameters for the RC specimens with different percentages of steel reinforcements.

	SPB1b	SPB2	SPB3
Percentage of tension steel (%)	1.45	1.06	0.75
Average loading rate (kN/s)	3.66	3.67	3.62
Load with respect to collapse load for loading cycle entering in heavy damage zone (%)	39.92	64.44	49.26
Residual deflection for loading cycle entering in heavy damage zone (mm)	3.90	4.80	3.8
Strain in steel for loading cycle entering in heavy damage zone	0.00322	0.0022	0.00203
Residual deflection just before failure (mm)	5.05	6.14	7.87
Deflection (for loading cycle entering in heavy damage Zone with respect to maximum deflection (%)	77.23	78.18	48.28
Strain (for loading cycle entering into heavy damage zone with respect to maximum strain (%)	79.12	66.67	95.77
Load cycle number first entered into heavy damage zone	52	44	33

6.4. Loading procedure

ACI 437-12 provides requirements for test load magnitudes, test protocols, and acceptance criteria for conducting a load test as a means of evaluating the safety and serviceability of concrete structural members [23]. And by following the same guidelines the loading pattern was applied on the RC flanged beam specimen (assumed as a RC girder in a bridge) as shown in Fig. 2a. The RC flanged beam specimen is subjected to loading protocol which has two types of pattern as shown in Fig. 2a. A series of service level load cycles are applied in between the load cycles of test trucks (TTs). These test trucks were chosen to represent the case of structural load testing in the *in-situ*. TTs were varied in loading magnitude. The smaller load repetitions are indicative of service level loads. From Fig. 2a one can observe that a series of TTs were repeated and the reason is to study the effect of loading repetitions on the AE response. The first phase of loading pattern has load intensity with relatively less peak and constitutes transport vehicle (TV) effect. The second pattern has higher peak load which constitutes elevated simulated test truck (ESTT). The two patterns together give single loading phase. Each loading phase has varying peak loads (Table 3).

7. Results and discussion

7.1. Mechanical response of RC flanged beams with different percentage of steel reinforcement in tension zone under flexural loading

The recorded load versus displacement and flexural strain in steel at mid-span plots are shown in Fig. 2b and c respectively. From Fig. 2d one can observe that the collapse load is increased due to increase in percentage of steel in the specimens, but the yield strain at collapse is same in all three cases.

The displacement at collapse is influenced by the percentage of steel reinforcement. Initially, displacement at mid-span continuously increased rapidly. The yielding of tensile steel is delayed due to increase in steel percentage. It also caused increase in the load carrying capacity and delays in development of flexural and shear cracks. Also the flexural strain in steel

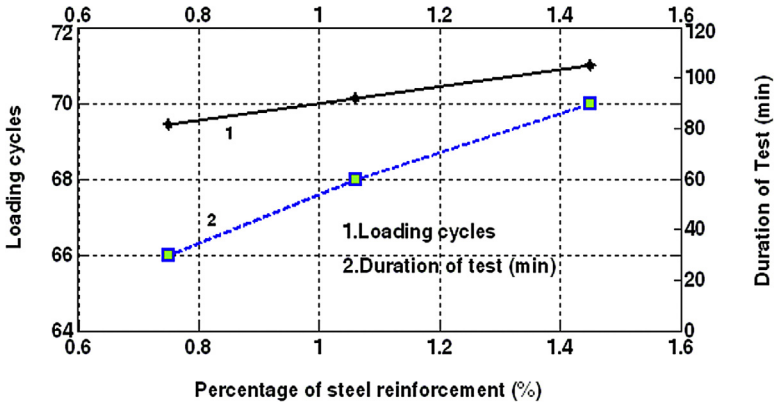

Fig. 3. Variation of number of loading cycles with percentage of steel reinforcement in the T-beam specimens.

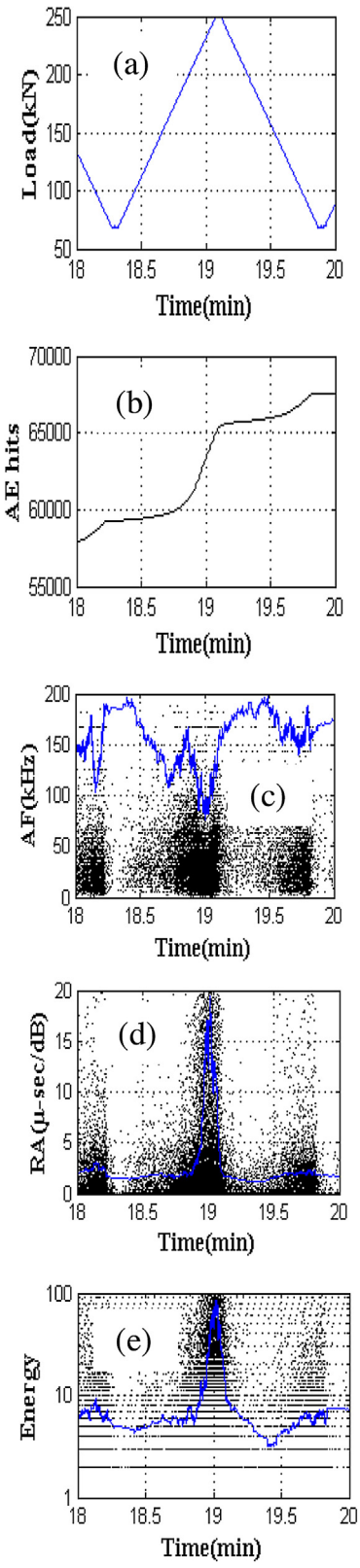

Fig. 4. Time history between 18 min to 20 min of (a) accumulated AE activity, (b) AF, (c) RA, and (d) AE energy for SPB1a RC flanged beam.

at collapse (0.00324) is less when compared to the yield strain of steel (0.0042) as per IS:456-2000, because the specimen was tested under incremental cyclic loading.

The time taken for the failure of the test specimen increased with an increase in percentage of steel. In an over-reinforced RC beam, steel does not yield but concrete crushes much before the collapse. The maximum number of loading cycles recorded till collapse are increasing as the percentage of steel is increased as evident from Fig. 3. Consequently the time taken for the failure (duration) is also increased. Thus it can be observed that the percentage of steel in the RC flanged beam specimens had influenced number of loading cycles. Because higher load is required to produce the same ultimate stress for larger area of cross section of steel (A_s). Since all the specimens tested under the same load cycles, to achieve a higher value of ultimate load greater duration was required as shown in Fig. 3. An increase of steel reinforcement from 0.8 percentage to 1.4 percentage (with a margin of 0.6 percentage) resulting additional increase in number of loading cycles and the test specimen endures nearly seventy more minutes. This observation gives the understanding on the increase in steel reinforcement in practical constructions.

7.2. AE characteristics of RC flanged beams with different percentage of steel reinforcement under flexural loading

Fig. 4c and d shows a moving average (window space equal to 100) of AF and RA value were plotted against time. It is observed that when there was sudden increase in load as shown in Fig. 4a, a large number of AE released is observed as shown in Fig. 4b. There has been a decrease in the average frequency (AF) and increase in the rise angle (RA) value. In Fig. 4c, with window space equal to 100, moving average of AF versus RA is plotted for SPB1a. During the early damage stage (corresponding to tensile mode) higher AF and lower RA are observed, while as the test specimen is led to final failure AF decreases and RA increases.

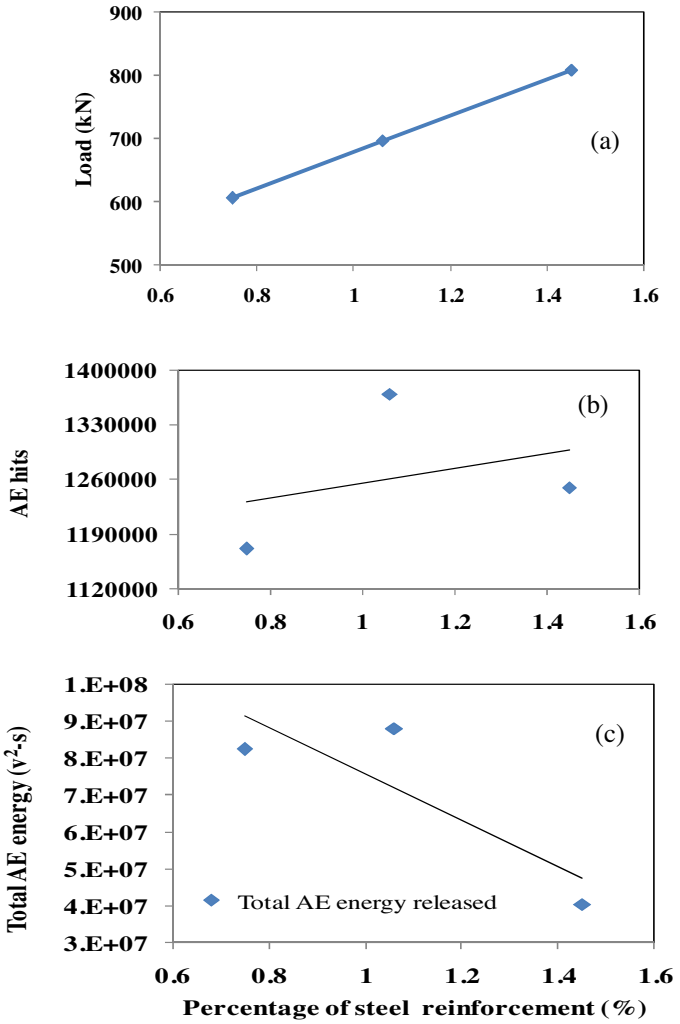

Fig. 5. (a) ultimate load and total AE hits recorded (b) AE hits and (c) AE energy with percentage of steel reinforcement in the T-beam specimens.

Fig. 5a shows a plot between ultimate load versus percentage of steel in the specimens. Load carrying capacity of the test specimen is high as the percentage of steel is more. Fig. 5b shows the total AE hits recorded versus percentage steel. Total recorded AE hits increases with the increase in percentage of steel. While the variation of AE hits recorded with the percentage of steel in specimen can be accounted to the fact that larger loads create several cracks, thus leading to increasing number of AE hits. The total AE energy released at collapse of the specimen with low percentage of steel is more when compared with the high percentage of steel as shown in Fig. 5c. As the stiffness of the test specimen is increased with increasing percentage of steel the AE energy released is reduced. The reason could be quick failure occurs in specimens made with very low percentage of steel. A slightly higher toughness may be the cause for the specimens with higher percentage tensile steel and this cause probably reduction in AE energy. When the steel percentage is less the test specimen is more

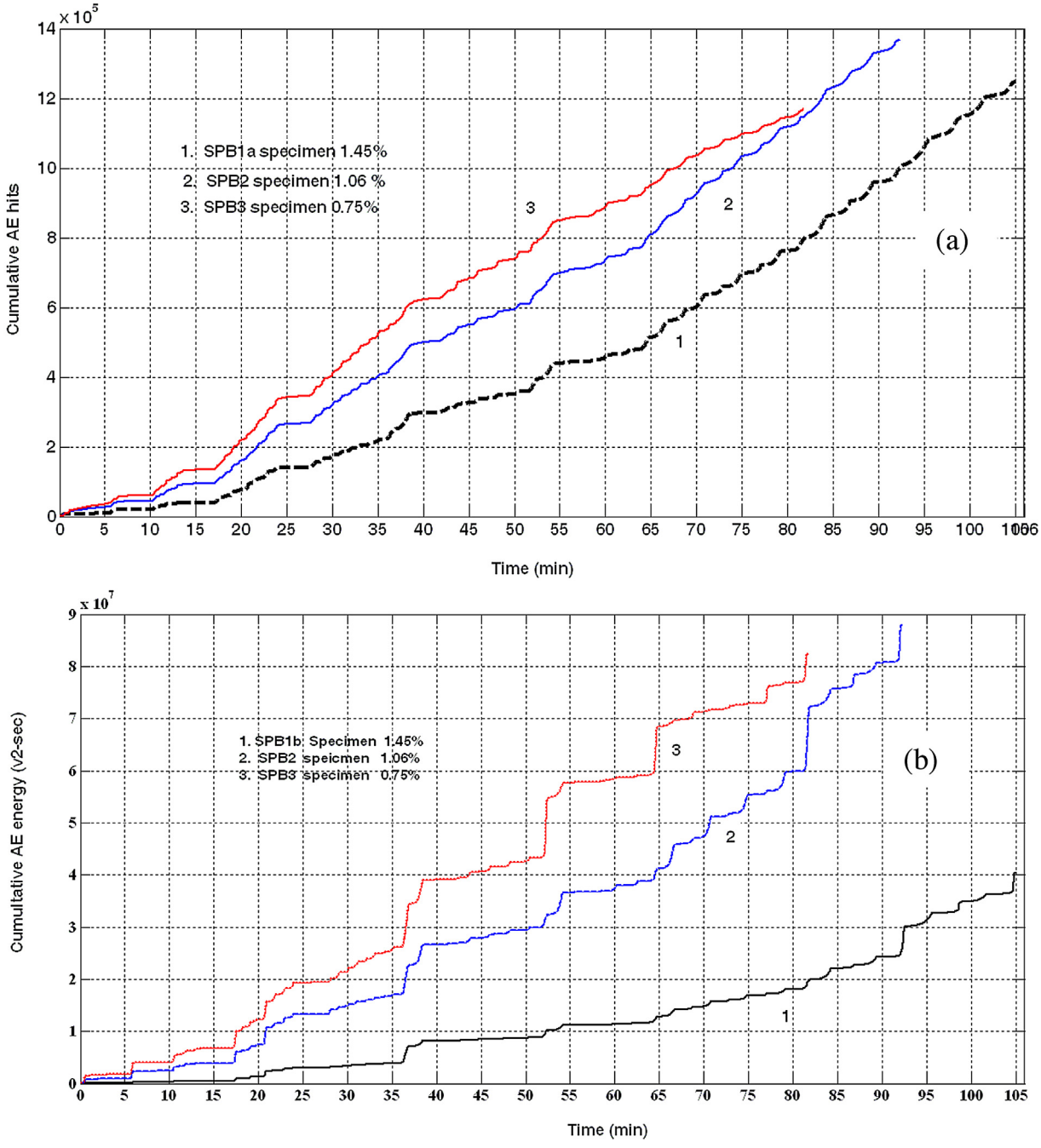

Fig. 6. Variation of (a) cumulative AE hits (b) cumulative AE energy with time.

ductile. The reason is steel attains maximum yield strain before collapse. But in case of specimens having high percentage steel, specimen does not attain yield strain before collapse, but failed due to maximum compressive strain in concrete.

Also brittleness of the specimen increases when the percentage of steel is more. A linear relationship could be possible between AE energy released and percentage of steel present in the RC beams. As percentage of steel increases AE energy released decreased as shown in Fig. 5c. A relation given in Eq. (1) has been proposed to obtain the percentage of steel (P) present in the RC beam by knowing the total AE energy released (AEER) till collapse.

$$\text{AEER} = -6 \times 10^{7P} + 10^{8} \tag{1}$$

Where p is the percentage of steel present in the RC test specimen under flexural loading. Fig. 6a and b shows variation of cumulative AE hits and energy released with time respectively. Higher percentage steel specimens depict lower slope of the line plotted between the cumulative AE hits recorded and percentage of steel. This indicates that energy released in specimens is low with higher percentage steel. In view of it's higher stiffness, bond between concrete and steel reinforcement, bending strength of RC member results less in released AE activity. The rise in AE energy is quicker in case of specimens made with lower percentage of steel. This indicates brittleness in the RC member and gives less warning at failure.

The total AE energy recorded at the collapse of the specimen is decreased as the reinforcement ratio is increased. Also from Fig. 6b, one can observe that the slope of the line plotted between cumulative AE energy and time for higher percentage

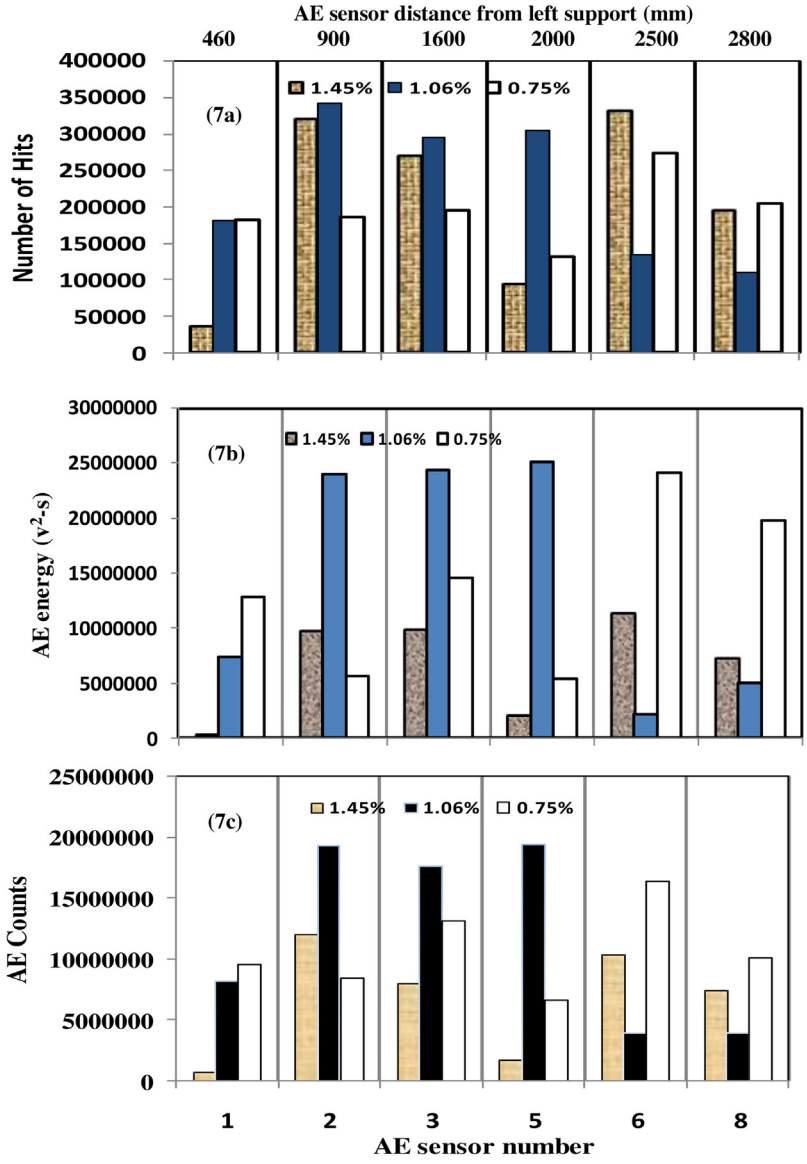

Fig. 7. (a) Number of AE hits (b) total energy and (c) total AE counts recorded at each channel (sensor) and distance.

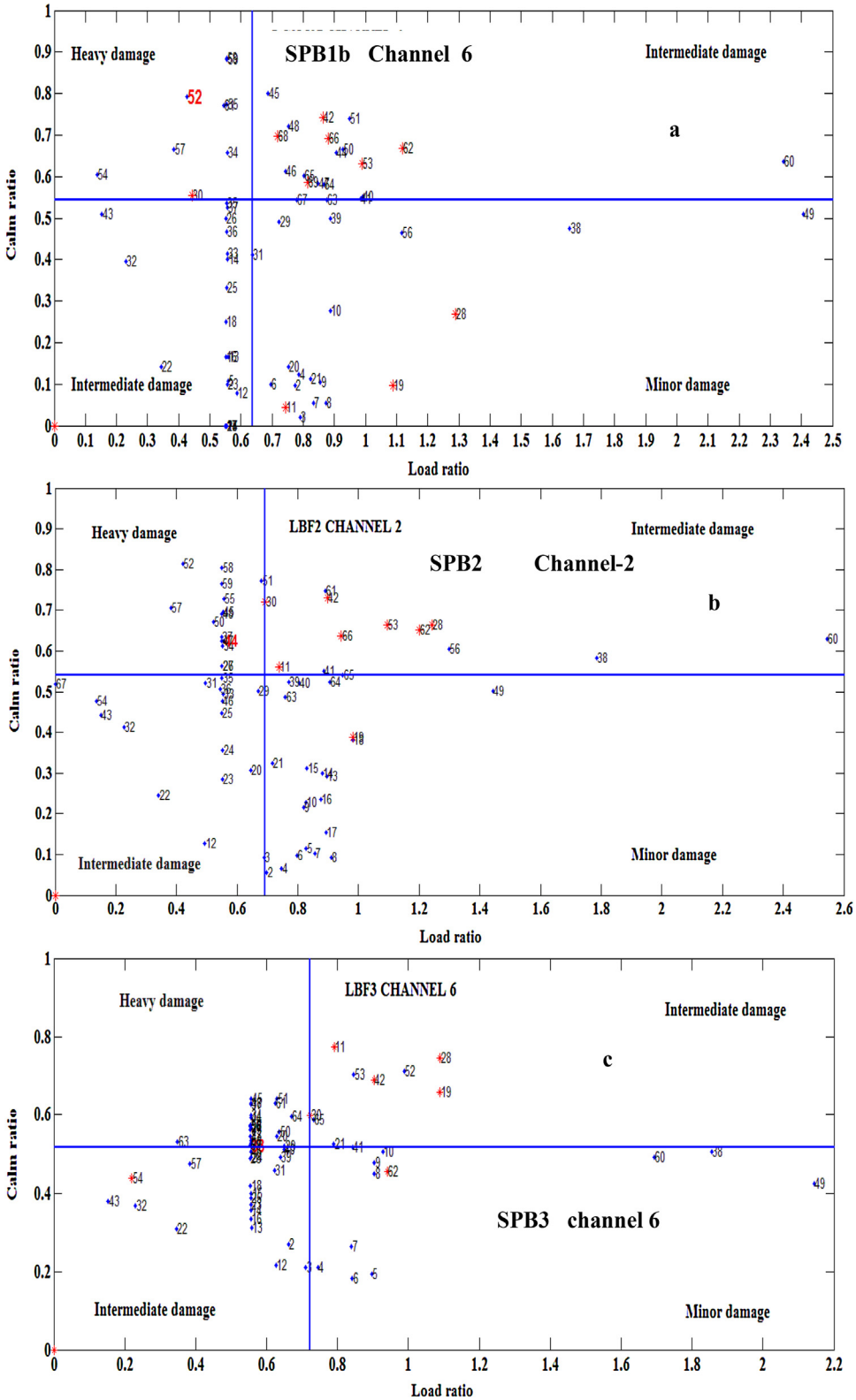

Fig. 8. Implementation of NDIS-2421 criterion for the RC beam specimens with 1.45 percentage of steel reinforcement [loading cycle 52 entered into heavy damage zone] [22]; b Implementation of NDIS-2421 criterion for the RC beam specimens with 1.06 percentage of steel reinforcement [loading cycle 44 entered into heavy damage zone] [22]; Implementation of NDIS-2421 criterion for the RC beam specimens with 0.75 percentage of steel reinforcement [loading cycle 33 entered into heavy damage zone] [22].

of steel is less when compared with lower percentage of steel. The reason could be when the reinforcement is more the specimen may behave more brittle in nature and fails quickly. When the percentage of steel reinforcement in the specimens increases the strain energy stored in the specimen gradually decreased because the yielding criteria predominantly dominate in high percentage steel specimen due to ductility. Because of this reason the strain energy release is lower as compare to brittle material, which gives clear distinction between low percentage specimen and high percentage steel specimen. This kind of phenomena while designing the RC specimen.

7.3. Identification of fracture process at a specific location in the RC structure using acoustic emission testing

The total number of AE hits recorded at each sensor is shown in Fig. 7a for three cases i.e, 1.45%., 1.06% and 0.75%. The X-distance of each AE sensor from left support is indicated on the top of the plot as shown in Fig. 7. In case of the specimen with 1.45 percentage steel, more hits were recorded at #Ch-2 and also at #Ch-6. This corresponds to the distance of 900 mm from the left support in X-direction. Also total AE energy and AE counts recorded is increased at # Ch-2 and #Ch-6. This indicates major cracking is taking place either near to Ch-2 or Ch-6 indicating at the supports. In case of specimens made with 1.06 percentage steel, the AE hits, energy and counts are more recorded in flexure at midspan, where #Ch-2, #Ch-3 and #Ch-5 are mounted. However, specimen made with 0.75 percentage steel, at #Ch-6 AE hits, energy and counts are recorded high near to the right support. This indicates major cracks occurred where more AE hits are present. The same pattern is observed in case of AE energy and AE counts as shown in Fig. 7b and c. One can identify the location of cracks based on AE parameter recorded versus sensor locations. It was observed that the source of AE signals appears that they are different in terms of AE amplitude depending on the source mechanism. AE activity is related to extent of damage. Therefore, the area near the sensor which recorded the highest AE activity is most likely to have more serious damage than the rest of the structure monitored.

7.4. Comparison with NDIS-2421 criterion for damage assessment

The damage taken place in the RC flanged beam specimens was studied with NDIS-2421 criterion [24–27]. To fix the limits for load ratio and calm ratio for assessment of damage as *minor*, *intermediate* and *heavy* in NDIS-2421 plot, a scattered point graph between load versus residual deflection (deflection at the end of each loading cycle) is plotted. Loading cycle is identified at the instant where the points (or residual deflections) are raised suddenly. The same loading cycle is considered for calculating limit for load ratio. Limit for the calm ratio is fixed based on the load and displacement at collapse [3,24–27]. Fig. 8a–c shows the corresponding NDIS-2421 assessment plots for test specimen SPB1b, SPB2 and SPB3 respectively. The load ratio limits are increased when there is a decrease in percentage of steel. As the percentage of steel present in the test specimen increased, the loading cycle number entering into the heavy damage zone also increased.

7.5. Crack classification in RC structures

JCMS-III B 5707 proposed a methodology for monitoring the crack propagation in RC structures [3,28]. This methodology uses AE parameters namely AF (=counts/duration) and RA (=rise time/peak amplitude) and the AE sources can be classified into tensile and shear cracks based on the relationship between AF and RA as shown in Fig. 9. But a defined criterion on the proportion of AF and RA is not established [28]. Also the AE recorded data is random in nature. Gaussian mixture modeling (GMM) is used to consider data distribution properties and to classify the AE data into two main clusters such as tensile and shear [28]. Fig. 10a–d shows GMM of feature vectors in SPB1b specimen. During the initial load steps, tensile cracks dominated. During intermediate load steps, a transition stage occurred. And at the final load steps, shear cracks dominated.

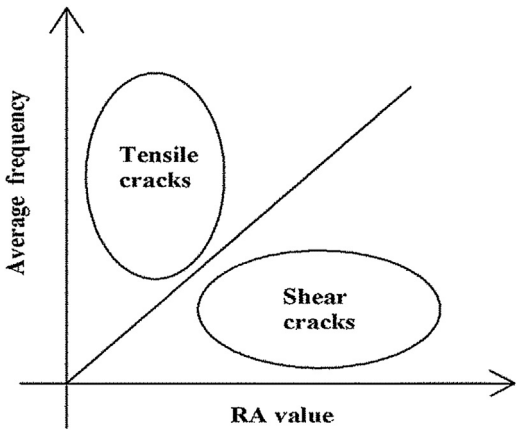

Fig. 9. Conventional crack classification in JCMS-III B 5706.

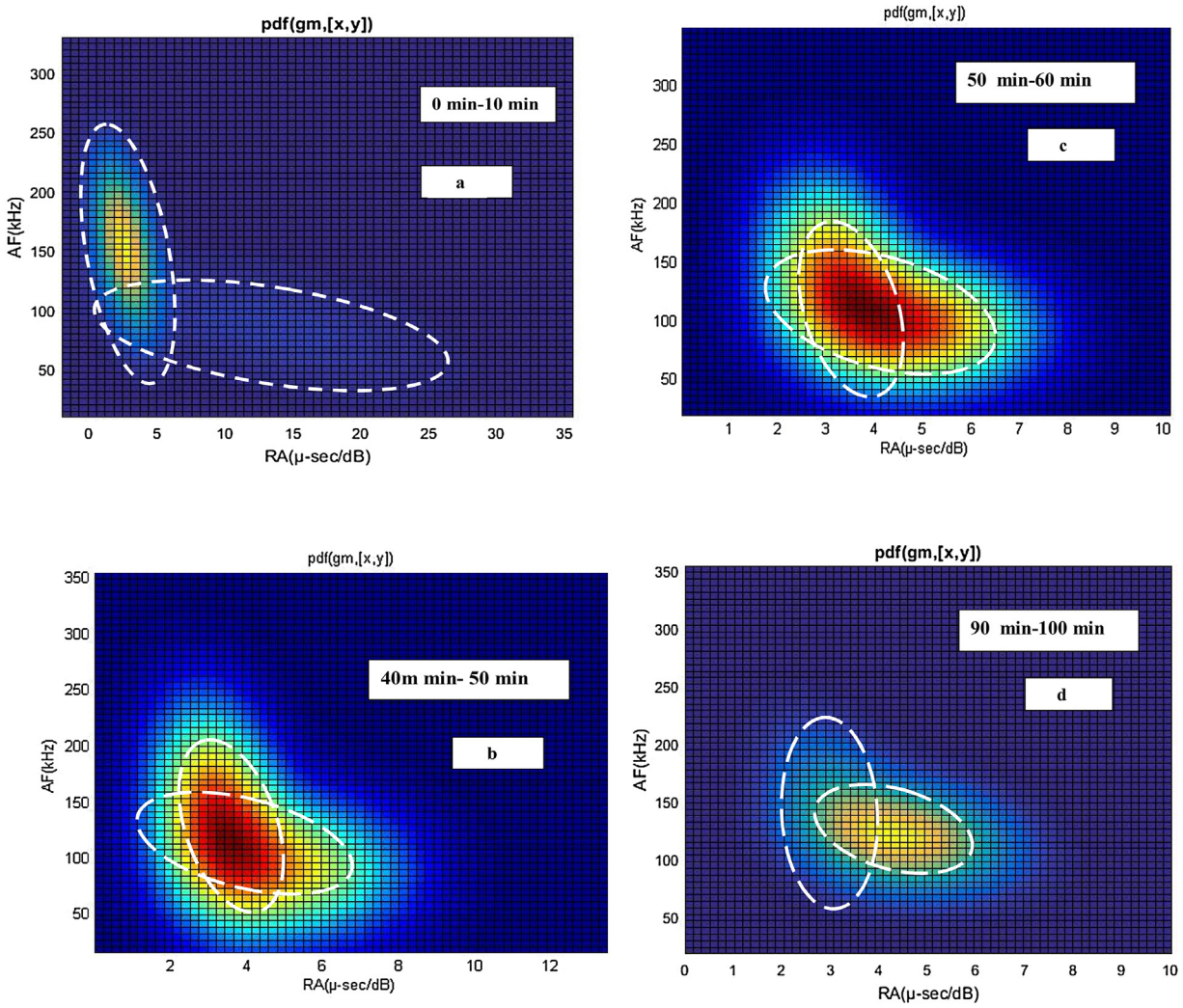

Fig. 10. GMM of feature vectors at various time interval for SPB1b specimen [28].

The AE data clusters having higher likelihood are classified into tensile or shear clusters and the common of the data is named as mixed. In case of specimen failed in flexure the transition state occurs in more time. The percentage of AE cluster is more in shear failure than in case of flexure failure. During the yielding region we will get the second highest peak, after the

Table 4
Percentage of AE activities for each time interval [28].

Time interval	Load step	AE hits			Tensile(%)	Shear(%)	Mixed(%)
		Tensile	Shear	Mixed			
0–10	1	6503	1906	145	76.02	22.28	1.70
10–20	2	14310	5306	254	72.02	26.70	1.28
20–30	3	2159	20875	86	9.34	90.29	0.37
30–40	4	7956	17730	290	30.63	68.26	1.12
40–50	5	4525	6455	1517	36.21	51.65	12.14
50–60	6	15589	6805	386	68.43	29.87	1.69
60–70	7	23072	6511	442	76.84	21.69	1.47
70–80	8	11568	21089	867	34.51	62.91	2.59
80–90	9	29497	8965	629	75.46	22.93	1.61
90–100	10	2924	52903	355	5.20	94.16	0.63

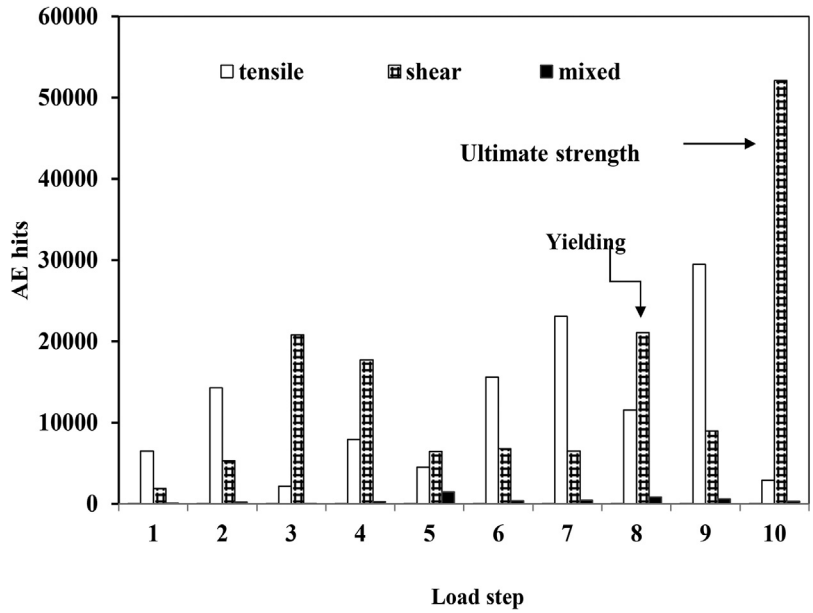

Fig. 11. Estimation of crack mode propagation by GMM algorithm in SPB1b specimen [28].

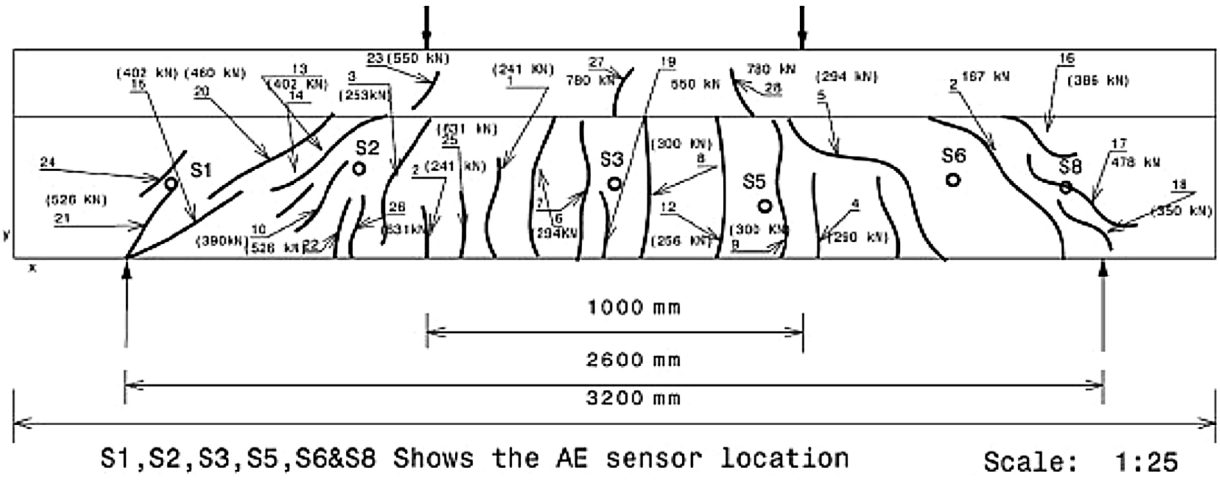

Fig. 12. Cracks developed after the experiment on the SPB1b specimen.

ultimate load phase. Table 4 shows the percentage of AE hits in each time interval. Fig. 11 shows the estimation of crack mode propagation. Fig. 12 shows the schematic representation of cracks developed on the test specimen. A percentage threshold of 62% for shear class seems reasonable in the case of specimen SPB1b.

8. Conclusions

Based on the above results the following major conclusions can be drawn.

1. Percentage of steel in the reinforced concrete structural member is an important factor that affects the released AE.
2. AE parameters such as hits recorded at a particular sensor advise the location in the RC structures where the damage is taking place.
3. Because of increase in brittleness in the test specimen due to high percentage of reinforcement steel, the total released AE energy decreased.

4. As the percentage of steel present in the test specimen increases, the loading cycle number entering into the heavy damage zone also increased.

Acknowledgement

This work was partially financially supported by the Bhabha atomic research center, Mumbai, India, Grant number SID/PC/99191.

References

[1] A. Carpinteri, E. Cadamuro, M. Corrado, Minimum flexural reinforcement in rectangular and T-section concrete beams, Struct. Concr. 15 (3) (2010) 361–372.
[2] IS:456:2000, Indian standard plain and reinforced concrete- code of practice., Bureau of Indian standards New Delhi 2000.
[3] C.U. Grosse, M. Ohtsu, Acoustic Emission Testing, Springer-Verlag, Berlin Heidelberg, 2008.
[4] M. Ohstu, Acoustic Emission and Related Non-destructive Evaluation Techniques in the Fracture Mechanics of Concrete – Fundamentals and Applications, Woodhead publishing limited, Sawston Cambridge, 2015.
[5] A. Behnia, H.K. Chai, T. Shiotani, Advanced structural health monitoring of concrete structures with the aid of acoustic emission, Constr. Build. Mater. 65 (2014) 282–302.
[6] M. Ohtsu, M. Uchida, T. Okamoto, S. Yuyama, Damage assessment of reinforced concrete beams qualified by acoustic emission, ACI Struct. J. 417 (2002) 411–417.
[7] S. Colombo, I.G. Main, M.C. Forde, Assessing damage of reinforced concrete beam using *b*-value analysis of acoustic emission signals, J. Mater. Civ. Eng. 15 (3) (2003) 280–286.
[8] R. VidyaSagar, M.V.M.S. Rao, An experimental study on loading rate effect on acoustic emission based *b*-values related to reinforced concrete fracture, Constr. Build. Mater. 70 (2014) 460–472.
[9] T. Schumacher, C. Higgins, S. Lovejoy, Estimating operating load conditions on reinforced concrete highway bridges with *b*-value analysis from acoustic emission monitoring, Struct. Health Monit. 10 (2011) 17–32.
[10] A. Ridge, P. Ziehl, Nondestructive evaluation of strengthened RC Beams: cyclic load test and acoustic emission methods, ACI Struct. J. 103 (6) (2006) 832–841.
[11] A. Nair, C.S. Cai, Acoustic emission monitoring of bridges: review and case studies, Eng. Struct. 32 (6) (2010) 1704–1714.
[12] S.W. Hearn, C.K. Shield, Acoustic emission monitoring as a nondestructive testing technique in reinforced concrete, ACI Mater. J. 94 (6) (1997) 510–519.
[13] D.J. Yoon, W.J. Weiss, S.P. Shah, Assessing damage in corroded reinforced concrete using acoustic emission, J. Eng. Mech. 126 (3) (2000) 273–283.
[14] C. Ouyang, E. Landis, S.P. Shah, Damage assessment in concrete using quantitative acoustic emission, J. Eng. Mech. 117 (11) (1991) 2681–2698.
[15] J.R. Watson, S. Yuyama, D. Johnson, Remote detection and assessment of damage in bridges, Proc Structural Faults and Repair Conf. (2001) (CD-ROM).
[16] S. Yuyama, S.T., Okamoto, T., Shigeishi, M., Ohtsu, T. Kishi, A proposed standard for evaluating structural integrity of reinforced concrete beams by Acoustic emissions, Acoustic emission: standards and technology update, ASTM, STP 1353, 1998, pp. 25–40.
[17] A. Benavent, E. Castro, A. Gallego, Evaluation of low-cycle fatigue damage in RC exterior beam-column subassemblages by acoustic emission, Constr. Build. Mater. 24 (2010) 1830–1842.
[18] A. Benavent-Climent, A. Gallego, J.M. Vico, An acoustic emission energy index for damage evaluation of reinforced concrete slabs under seismic loads, Struct. Health Monit.- Int. J. 11 (2012) 69–81.
[19] F.A. Sagasta, A. Benavent-Climent, A. Roldán, A. Gallego, Correlation of plastic strain energy and acoustic emission energy in reinforced concrete structures, Appl. Sci. 6 (2016) 84.
[20] M. Abadelrahman, M.K. Elbatanouny, P.H. Ziehl, Acoustic emission based damage assessment method for prestressed concrete structures: modified index of damage, Eng. Struct. 60 (2014) 258–264.
[21] A. Larosche, P. Ziehl, J. Mangual, M.K. ElBatanouny, Damage evaluation of prestressed piles to cast in place bent cap connections with acoustic emission, Eng. Struct. 84 (2015) 184–194.
[22] R. Vidya Sagar, A parallel between earthquake sequences and acoustic emissions released during fracture process in reinforced concrete structures under flexural loading, Constr. Build. Mater. 114 (2016) 772–793.
[23] American concrete institute (ACI), Code requirements for load testing of existing concrete structures, ACI committee, Farmington hills, MI,ACI 437-12, (2012) 34.
[24] S. Colombo, M.C. Forde, I.G. Main, J. Halliday, M. Shigeishi, AE energy analysis on concrete bridge beams, RILEM Mater. Struct. 38 (2005) 851–856.
[25] R. VidyaSagar, B.K. Raghu Prasad, R.K. Singh, Kaiser effect observation in reinforced concrete structures and its use for damage assessment, Arch. Civil Mech. Eng. 15 (2) (2015) 548–557.
[26] K.M. Holford, Acoustic emission – Basic principles and future directions, Strain 36 (2) (2000) 51–54.
[27] Japanese Society for Nondestructive Inspection, Recommended Practice for In Situ Monitoring of Concrete Structures by Acoustic Emission, JNIS-Publication, Japan, 2000.
[28] A. Fardizadeh, S. Salamone, P. Singh, A probabilistic approach for damage identification and crack mode classification in reinforced concrete structures, J. Int. Mat. Sys. Str. 24 (14) (2013) 1722–1735.